ACS APPLIED MATERIALS & INTERFACES

Research Article

www.acsami.org

Dispersed CuO Nanoparticles on a Silicon Nanowire for Improved Performance of Nonenzymatic H_2O_2 Detection

Jianfei Huang, Yihua Zhu,* Hua Zhong, Xiaoling Yang, and Chunzhong Li*

Key Laboratory for Ultrafine Materials of Ministry of Education, School of Materials Science and Engineering, East China University of Science and Technology, 130 Meilong Road, Shanghai 200237, China

Supporting Information

ABSTRACT: A finely dispersed CuO nanoparticle electrocatalyst on a silicon nanowire (SiNW) was achieved via a designed, precursor-mediated strategy by combining metal-assisted chemical etching, electroless deposition, and thermal oxidation. The CuO assembled on silicon nanowires (CuO-SiNWs) showed a competent sensitivity of 22.27 μA/mM, a wider linear range from 0.01 to 13.18 mM, and a comparable detection limit of 1.6 μM (3S/N) for nonenzymatic H_2O_2 detection. The archetype sensor also demonstrated eligible selectivity against common interfering species. By the introduction of the SiNW carrier, which led to mitigated conglomeration of the electrocatalyst and a favorable microstructure of the electrocatalyst−carrier system, improved signal-concentration linearity and higher electrocatalyst utilization efficiency were obtained with CuO-SiNWs. These results demonstrated the feasibility of the synthetic strategy and the potential of the nanocomposite as a promising candidate for H_2O_2 sensing.

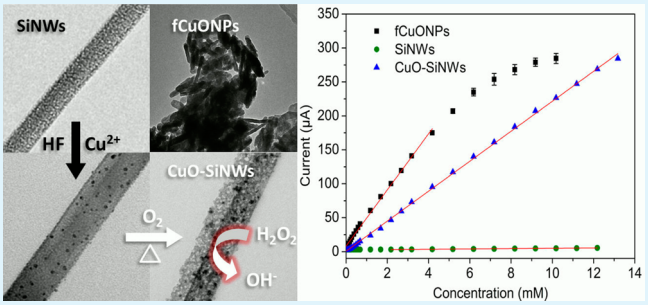

KEYWORDS: *silicon nanowire, mitigated conglomeration, cupric oxide, precursor-mediated, hydrogen peroxide, nonenzymatic sensor*

INTRODUCTION

Owing to the wide applications of hydrogen peroxide (H_2O_2) in industrial fields[1] and its significance in biological study,[2] efficient and reliable detection of H_2O_2 is essentially important. While various enzyme-based H_2O_2 biosensors were developed,[3−5] their utility is commonly debased by the high costs of enzymes, complex electrode fabrication, and performance instability.[6] Recently, the development of nonenzymatic H_2O_2 sensors has aroused wide research interest. Narang et al.[7] constructed a gold electrode modified with multiwalled carbon nanotubes (MWCNT) and Au nanoparticles as a nonenzymatic sensor for H_2O_2. Xiao et al.[8] prepared Au−platinum (Pt) alloy nanoparticles on an ionic liquid−chitosan film and achieved nonenzymatic H_2O_2 detection at submicromolarity. Although H_2O_2 sensors based on noble metals showed comparable performance, they are not economically ideal considering the hiking costs and limited resources of noble metals. While silver (Ag) seems acceptable in terms of costs, nanosized Ag generally suffers from instability.[9] Among other alternatives, cupric oxide (CuO) stands as a good candidate because of its fascinating electrochemical properties and cost-effectiveness. Successful attempts have been made to prepare nanosized electroactive CuO for chemical sensing,[10−13] yet for all that, efficient utilization of CuO electrocatalysts for sensing application still demands further effort for structural optimization aiming at facilitated analyte diffusion, large surface areas, and good charge/electron transfer from electrocatalysts to the modified electrodes.

The preparation of electrocatalysts at nanosize leads to larger surface areas and more accessible active sites and nanosized electrocatalysts promote electrode kinetics compared with their bulk counterparts.[14] Nevertheless, efficient utilization of nanosized catalysts is usually challenged by undesirable conglomeration, where large surface areas and abundant active sites are lost and thus the performance is undermined. As a solution, a catalyst−carrier system can be designed. For example, Shuai et al.[15] realized a Pd/carbon nanofiber nanocomposite for enhanced nitrite reduction. Nickel nanoparticles formed on graphene platelets were proposed for Pt catalyst-free dye-sensitized solar cells by Bajpai et al.[16]

As an attractive one-dimensional nanomaterial featuring source abundance, promising scalable production, biocompatibility, and readiness for the semiconductor industry, silicon nanowire (SiNW) has also been explored as a carrier or synergetic support in photoelectrochemical cells,[17] sensors,[18] SERS substrates,[19] and pollutant degradation,[20] holding promise as a versatile supporting material. While metal deposition and grafting of organic groups onto a SiNW carrier were common, reports concerning the integration of nanostructured metal oxides onto SiNW have been relatively fewer despite the rich functionality offered by them. Loading metal oxides onto SiNW usually requires chemical vapor deposition,[21] atomic layer

Received: November 20, 2013
Accepted: May 6, 2014
Published: May 6, 2014

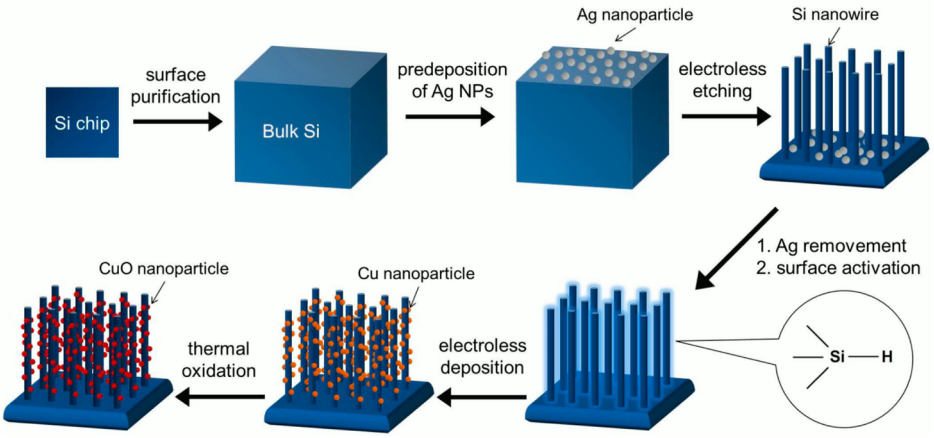

Figure 1. Schematic illustration of the synthesis of the CuO-SiNW nanocomposite.

deposition,[22] and sputtering.[17] The drawback of these techniques is that gas-phase reaction, costly devices, special reagents, complex manipulations, and extreme conditions are often involved. Thus, it remains challenging to develop facile assembly protocols to integrate nanosized metal oxides onto SiNW. Recently, Au nanoparticles have been assembled onto TiO_2 nanowires in a solution-based method by anchoring the $AuCl(OH)_3^-$ complex on the nanowire surface as a precursor.[23] Inspired, we proposed a precursor-mediated strategy to facilely prepare metal oxides supported on SiNW, where a connection should be previously made between a precursor and SiNW in a solution milieu. Subsequently, the precursor can be accordingly transformed to the target oxide. Because the surface of SiNW can be treated into a OH-, H-, Cl-, or NH_2-terminated layer,[24] we predicted that it will benefit the fixation of various precursors through hydrogen bonding, electrostatic action, coordination bonding, or chemical reaction.

Herein, a nanosized CuO electrocatalyst assembled onto silicon nanowire (CuO-SiNW) was realized through the described synthetic strategy. The overall synthetic procedure is schematized in Figure 1. Cu was chosen as the precursor for a simple approach to metallized SiNW has been systematically studied.[25] The Cu nanoparticles grown on the SiNW were completely transformed to CuO nanoparticles by dry oxidation. In addition to the excellent performance for nonenzymatic H_2O_2 detection, the designed CuO nanoelectrocatalyst−SiNW system demonstrated improved efficiency of the electrocatalyst and linearity of the archetype sensor.

EXPERIMENTAL SECTION

Reagents and Chemicals. The silicon (Si) wafers (p-type, 100-faceted, 0.1−1 Ω cm) were bought from Zhejiang Lijing Materials Technology Co. Ltd. Ascorbic acid (AA), uric acid (UA), and Nafion were purchased from Alfa Aesar. All other chemicals were purchased from Lingfeng Chemical Reagent Co. Reagents were used as received without further purification. Water used in all experiments was ultrapure (18 MΩ cm).

Preparation of SiNW. The preparation of the SiNW was conducted according to a metal-assisted etching protocol similar to a previous work.[26] Briefly, Si wafer chips (cut into 1 × 1 cm^2) were cleansed by successive sonication in ethanol and acetone for 15 min and treated with a "piranha" solution (H_2SO_4:30% H_2O_2 = 3:1, v/v) to purify the surface. Subsequently, the chips were immersed in a HF solution (5%) for 5 min to obtain a hydrogen (H)-terminated surface. Then, the chips were dipped into a solution of $AgNO_3$/HF (4.8 M/0.005 M) for 1 min. Rinsed with deionized water to remove Ag^+ ions, the chips were immediately transferred to an etchant solution containing 4.8 M H_2O_2 and 0.3 M HF. After etching for 40 min, a dilute HNO_3 solution (1:1, v/v) was used to remove Ag catalyst for 1 h. Then the chips were rinsed with deionized water several times and dried under a gentle nitrogen flow.

Formation of CuO Nanoparticles on SiNWs. The Si chips with SiNW arrays on the surface were first treated with HF (5%) to remove surface oxide formed in the dilute HNO_3 solution and rinsed with deionized water. Afterward, they were immersed in a 1 mM $CuSO_4$ solution for 15 min, during which Cu^{2+} ion was reduced to form a Cu nanoparticle precursor on the SiNWs. After rinsing with deionized water and drying under a vacuum, the Cu precursor supported on SiNWs was subjected to a thermal treatment of 500 °C in air, where the Cu was completely oxidized to CuO.[27]

Construction of the Working Electrode. The working electrode was fabricated using a glassy carbon electrode (GCE) modified with the as-prepared CuO-SiNWs (CuO-SiNWs/GCE). In particular, the GCE was successively polished with an aqueous slurry of alumina powder with sizes of 1 and 0.05 μm and dried in nitrogen before use. The CuO-SiNWs were collected by scratching the chip surface. A 10 μL ethanol suspension of 3 mg/mL CuO-SiNWs containing 0.5 wt % Nafion was dropped onto the surface of the polished GCE to be allowed to dry under ambient conditions. Working electrodes of all control groups were also thus fabricated except that the CuO-SiNWs were accordingly replaced.

Characterization and Electrochemical Measurements. Characterization of the as-prepared materials was conducted using field-emission scanning electron microscopy (FE-SEM; S4800) and transmission electron microscopy (TEM; JEM 2011 JEOL, Japan) with energy-dispersive X-ray spectroscopy (EDS). X-ray diffraction (XRD; Rigaku D/MAX 2550 VB/PC, Japan) was applied to investigate the crystalline structure of the nanocomposite. All electrochemical measurements were carried out with an electrochemical workstation (CHI660, Shanghai Chenhua Co.) under a conventional three-electrode configuration employing Pt, AgCl/Ag (saturated by a KCl solution), and CuO-SiNWs/GCE as the counter, reference, and working electrodes, respectively. For amperometric tests, a transient background current at the beginning of the tests was allowed to decay to a steady state before the addition of analytes.

RESULTS AND DISCUSSION

The as-prepared SiNW arrays rendered the Si wafer chip a black and dull surface in accordance with a previous report.[28] This is because of light trapping caused by the dense nanowire array structure, which can be observed by a microstructure study of the Si wafer chip. Parts a and b of Figure 2 present typical cross-sectional SEM images of the as-prepared SiNW arrays in the side and tilt views. The vertically aligned SiNW arrays densely standing on the Si substrate are about 12 μm in length. The actual length of the nanowires for electrode fabrication is generally

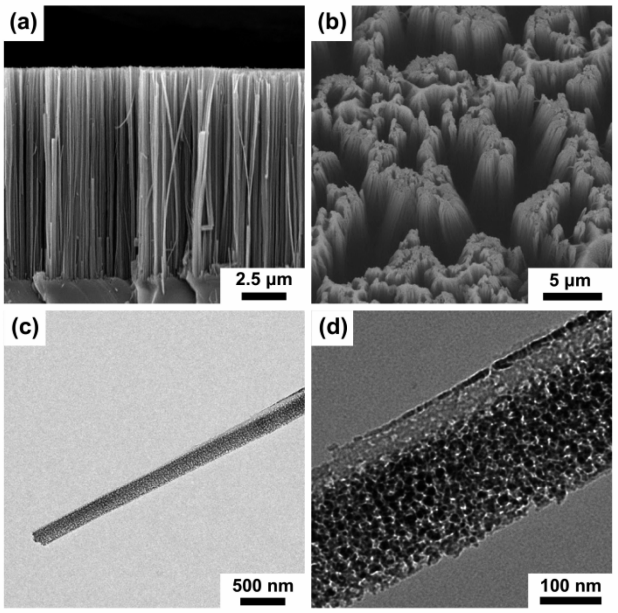

Figure 2. SiNWs presented in the side (a) and tilt (b) views of the SEM images and TEM images of a single SiNW (c) and its magnified part (d) for observation of the porous structure.

shorter because of the doctor-blade method used for collection of the nanowires. The morphology of the nanochannel-like space between parallel nanowires is favorable for further chemical modification because reagent species can diffuse conveniently and come into contact with the whole length of the SiNWs. Unlike free SiNWs prepared under the vapor-liquid-solid (VLS) mechanism, SiNWs formed in the wet chemical etching process showed little dependency of the diameter on the synthetic parameters and their diameters often cover a range of up to 200 nm.[26,28] As is shown in the TEM image of Figure 2c, a single SiNW is photographed. Moreover, its magnified TEM image in Figure 2d reveals a random porous structure of the nanowire with a pore size of around 10−20 nm. This porous structure may be beneficial in applications that demand the favorable diffusion of solutes. The formation of SiNW arrays and the porous structure has been discussed elsewhere.[29]

When the Ag nanocatalyst for chemical etching was removed by HNO_3, an oxide layer was simultaneously formed. This oxide layer was relatively inert, so surface activation was conducted using 5% HF to dissolve the surface oxide and form a H-terminated surface with stronger reducibility. In the ensuing electroless deposition process, Cu^{2+} ions were reduced by the H−Si surface to form a Cu precursor. Subsequently, this precursor, which was subjected to thermal treatment, underwent a transformation to CuO nanoparticles, during which a firmer connection was simultaneously made between the particles and nanowire by thermal annealing. A SEM image in a distant view of the CuO-SiNWs is presented in Figure 3a, from which no significant morphological change of SiNWs is observed, evidencing good stability of the SiNW in antecedent synthetic conditions. Figure 3b is a close-up view of Figure 3a exhibiting CuO particles attached on the Si nanowire surface. The results of TEM characterization, as can be seen in Figure 3c,d, further affirm the successful decoration of uniformly distributed Cu nanoparticles and CuO nanoparticles on the SiNW, respectively. In Figure 3e, several roughly parallel CuO-decorated SiNWs were photographed, with the porous structure of the nanowire

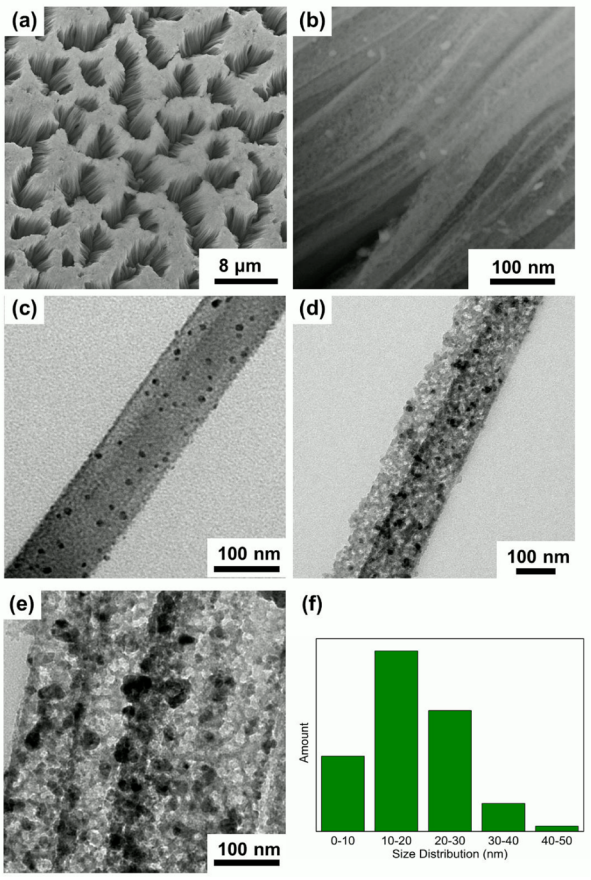

Figure 3. SEM images of the CuO-SiNW arrays in a distant view of a tilting angle of 75° (a) and a close-up view of the nanowire sidewall (b). TEM images of a single Cu-decorated SiNW (c) and CuO-SiNW (d). (e) Close-up view of the porous structure of CuO-SiNW. (f) Particle-size distribution of CuO particles.

preserved according to the contrast (black for CuO, gray for the SiNW, and mottled white for the pores). This is thanks to the low concentration of Cu^{2+} and the controlled deposition time that prevented overgrowth of the Cu nanoparticles from covering the whole surface of the nanowires. The size of the CuO particles mainly covers a range of 10−30 nm, as is shown in Figure 3f. The preparation of nanoparticles in situ on/in carriers can lead to the fine distribution of nanoparticles and suppressed particulate conglomeration,[30,31] while the direct synthesis of nanoparticles without carriers may result in undesirable conglomeration. Figure SI 2 in the Supporting Information (SI) shows the TEM image of seriously conglomerated rodlike CuO nanoparticles prepared by a solid-phase reaction. Visual contrast between the two kinds of CuO nanoparticles typically suggests the advantage of introducing carriers for uniform particulate distribution.

To further confirm the successful formation of the CuO electrocatalyst, analysis by EDS and XRD was carried out. The EDS pattern of the CuO-SiNWs in Figure 4a shows the peaks of Si, Cu, and oxygen (O) in correspondence to the presence of SiNWs and copper oxides, respectively. The peaks of Cu and O are unlikely to come from Cu_2O because thermodynamic calculation (see the SI) reveals the impossibility for the formation of Cu_2O under our synthetic configurations. Also, in the XRD pattern in Figure 4b, although the intensity of the diffraction peaks of CuO is quite low compared to the strong one of Si, the diffraction peaks between 30 and 40° corresponding to (110),

dx.doi.org/10.1021/am501799w | ACS Appl. Mater. Interfaces 2014, 6, 7055−7062

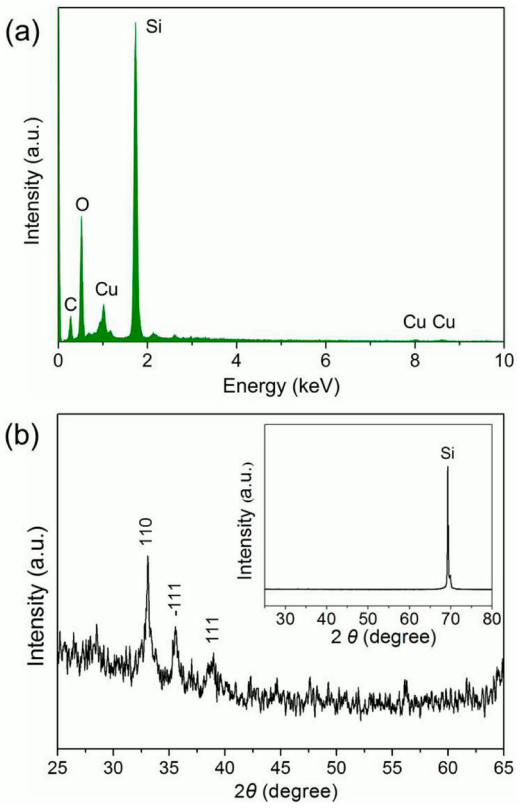

Figure 4. EDS (a) and XRD (b) patterns of CuO-SiNWs. The inset of part b is the XRD pattern with a wider 2θ range.

(−111), and (111) facets of monoclinic CuO are still apparent. With the absence of the diffraction peaks of Cu and Cu_2O, complete transformation from Cu to CuO in dry oxidation can thus be confirmed.

The electrochemical properties of the CuO-SiNWs/GCE were evaluated via cyclic voltammetry (CV) in a 0.1 M phosphate buffer solution (PBS; pH = 7.0) at a scan rate of 50 mV/s. In Figure 5a, when H_2O_2 is absent, two reduction peaks at −0.18 and −0.3 V can be seen, which are ascribed to the reduction process from Cu^{II} to Cu^{I} and from Cu^{I} to Cu^{0}, respectively. For PBS containing 1 and 2 mM H_2O_2, a significant increase in the reduction current is displayed, with the reduction peak at −0.3 V almost overlapped by a plateau of the increased reduction current as the overpotential shifts negatively, typically indicating electrocatalytic reduction of H_2O_2. To make a sound confirmation on which of the component contributed to the electrocatalytic reduction, control tests were also performed. Parts b and c of Figure 5 show the cyclic voltammograms of Nafion-modified GCE and SiNW-modified GCE (SiNWs/GCE) under the same experimental configurations. Obviously, for all of the control groups, the presence of 2 mM H_2O_2 only causes a slight increase of the reduction current, with no discernible shape change of the CV curves. This fairly confirms the electrocatalytic behavior toward H_2O_2 reduction as the contribution of CuO nanoparticles. Moreover, a comparison can also be made between the cyclic voltammograms of CuO-SiNWs/GCE and the control groups with 2 mM H_2O_2 to see a significant positive shift of the reduction starting overpotential to −0.08 V from −0.3 V in the control tests. This further manifests the improved electrocatalytic reduction of H_2O_2 resulting from the CuO electrocatalyst. CV with scan rates varying from 10 to 100 mV/s was used to further investigate the electrode reaction

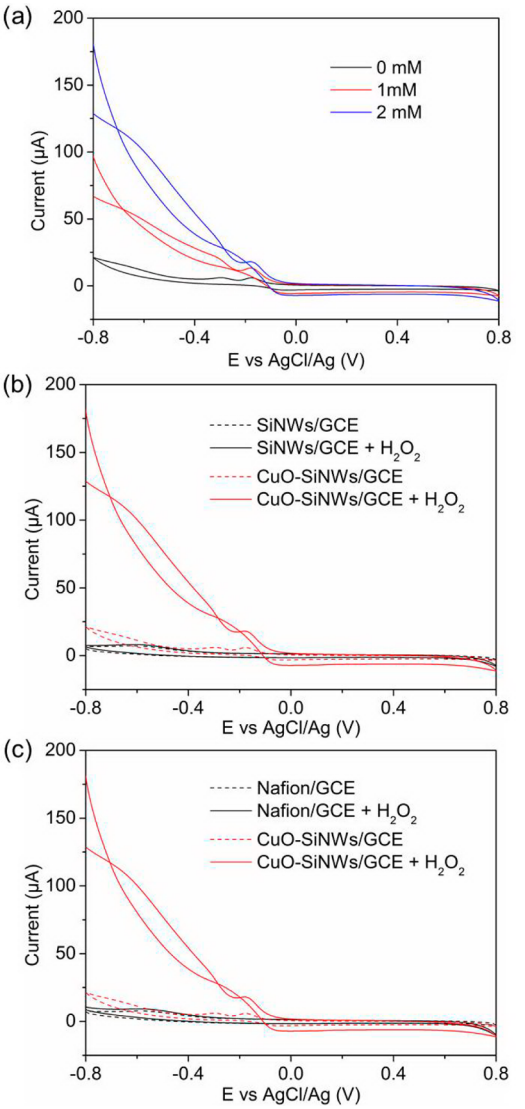

Figure 5. CV of CuO-SiNWs/GCE (a) in a 0.1 M PBS (pH = 7.0) containing 0, 1, and 2 mM H_2O_2 and in comparison to Nafion/GCE (b) and SiNWs/GCE (c) in 0.1 M PBS (pH = 7.0) containing 0 and 2 mM H_2O_2.

process, as is shown in Figure 6. In Figure 6b, the peak current increases linearly with the scan rate, suggesting a surface-adsorption-controlled process, which is similar to the previous work.[32] Comprehensively, from the above results, a proposed mechanism of the electrocatalytic reduction of H_2O_2 via CuO-SiNWs/GCE is depicted in Figure 7.

Amperometric i−t tests were conducted to evaluate the H_2O_2 detection performance of the CuO-SiNWs/GCE. For eclectic consideration on sensitivity and possible interference at high overpotentials (see the SI), an applied potential of −0.4 V situated at the plateau of the increasing reduction current was chosen, although the current peak seems to appear around −0.6 V. Figure 8a displays the current response of the CuO-SiNWs/GCE upon the successive addition of H_2O_2 to a solution of 0.1 M PBS (pH = 7.0) under magnetic stirring. As is shown, the current rapidly increases in response to each addition of H_2O_2, presenting a stairlike curve. The inset of Figure 8a is a magnified current curve at low concentrations, showing a stepwise increase in accordance with H_2O_2 addition and a fast response to analyte addition, where the current reaches a steady status in about 1.5 s.

dx.doi.org/10.1021/am501799w | ACS Appl. Mater. Interfaces 2014, 6, 7055−7062

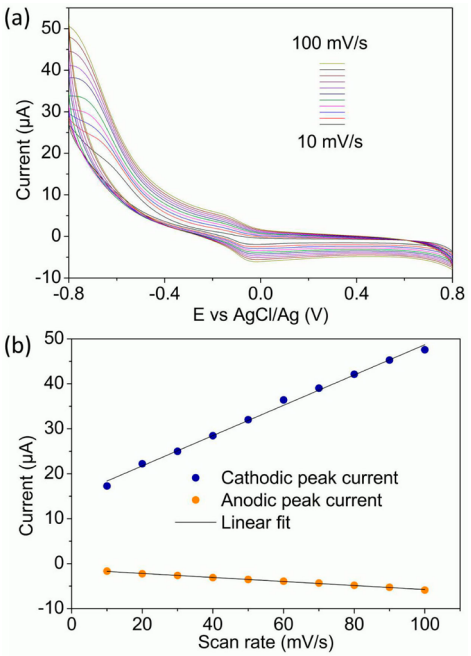

Figure 6. (a) CV of CuO-SiNWs/GCE at scan rates varying from 10 to 100 mV/s (10 mV/s every interval) in PBS (pH = 7.0) containing 0.1 mM H_2O_2 and (b) the corresponding calibration plot.

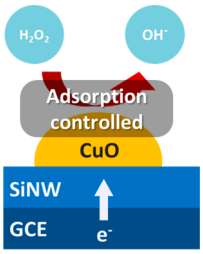

Figure 7. Mechanism for H_2O_2 detection based on CuO-SiNWs/GCE.

This fast response is likely due to favored analyte diffusion through the porous structure of the SiNW as well as uniform dispersion of the CuO electrocatalyst. As was confirmed in previous CV tests, the response toward H_2O_2 addition arose from electrocatalytic reduction effects from CuO. To further investigate the synergetic effect of the SiNW carrier and CuO electrocatalyst on the detection performance, control groups of two GCEs respectively modified with free CuO nanoparticles (fCuONPs/GCE) and SiNWs (SiNWs/GCE) were also constructed as working electrodes for amperometric $i-t$ tests (for experimental details, see the SI). The amperometric $i-t$ curves of the control groups and calibration plots of all three working electrodes are shown in parts b and c of Figure 7, respectively. On the basis of the Origin data analysis software, the linear regression equations and linear range of the (1) CuO-SiNWs/GCE, (2) fCuONPs/GCE, and (3) SiNWs/GCE are as follows:

$$I\ (\mu A) = 0.58523 + 22.07362C_{H_2O_2}\ (R^2 = 0.9994);\ 0.01-13.18\ mM \quad (1)$$

$$I\ (\mu A) = 8.25943 + 41.33948C_{H_2O_2}\ (R^2 = 0.9965);\ 0.01-4.18\ mM \quad (2)$$

$$I\ (\mu A) = 2.62366 + 0.23286C_{H_2O_2}\ (R^2 = 0.9961);\ 1.18-12.18\ mM \quad (3)$$

As proven by its flat $i-t$ curve and calibration plot with an extremely low sensitivity of 0.23 μA/mM, the current response of the SiNWs/GCE toward analyte addition was inconsequential, fitting previous CV tests. In fact, as is illustrated in Figure 7d and the inset of Figure 7b, the SiNWs/GCE produced no appreciable response and stairlike current curve until a total H_2O_2 concentration of 1.18 mM was reached, which also suggests dispensable consideration for the current response generated from SiNW−analyte interaction. Differently, the fCuONPs/GCE demonstrated CV curves (Figure SI 3 in the SI) and current response similar to those of the CuO-SiNWs/GCE, again confirming the electrocatalytic ability CuO. Notably, the fCuONPs/GCE showed a higher sensitivity than the CuO-SiNWs/GCE. This is because the fCuONPs/GCE containing CuO of the same weight as CuO-SiNWs can take advantage of its 100% mass fraction of the CuO electrocatalyst over a presumably low CuO/Si ratio in CuO-SiNWs, thus displaying a higher apparent sensitivity. This is similar to the report[33] where a higher payload of the electrocatalyst may result in higher sensitivity (but a narrowed linear range). According to the mass fraction of Cu measured by EDS, the mass fraction of CuO in CuO-SiNWs is preliminarily estimated to be 2.39%. Hence, much higher specific current response from the electrocatalyst, namely, a higher electrocatalyst usage efficiency, is achieved by the CuO-SiNWs. To realize a comprehensively improved performance, it is necessary to strike a balance between the payload of the functional elements and the efficiency of the electrocatalyst efficiency by finely adjusting the synthetic parameters, which demands further investigation and optimization. Considering their sensitivity of the same order of magnitude, the CuO-SiNWs/GCE is not inferior to fCuONPs/GCE in practical applications because current amplification is common in sensing devices. On the contrary, the fCuONPs/GCE without SiNWs as carriers showed irremediable drawbacks in terms of its linearity of the current−concentration relationship: Even with a lower correlation coefficient (R^2), the linear range is still narrower compared to that of the CuO-SiNWs/GCE. The decreased upper linear limit is also reflected in its decaying $i-t$ curve at high analyte concentrations, from which saturation of the analyte at active sites is inferred. For the CuO-SiNWs/GCE with a much wider linear range of 0.01−13.18 mM, unsaturation of the analyte at high concentrations as reflected by its current curve resulted from the suppressed conglomeration of the CuO electrocatalyst and thus the preservation of abundant active sites. Except for the mitigation of electrocatalyst conglomeration, SiNWs can form a network in the Nafion film, building a bridge that shuttles electrons between CuO and the GCE. In addition to the network architecture adopted for the nanocomposite, vertical alignment of the one-dimensional nanomaterial may also be of interest because the unique well-aligned form is quite different from the nanowire network, which may incite further investigation.[34] Besides, the porous structure in the SiNW can benefit diffusion of analyte molecules. With multiple advantages, an excellent detection performance is therefore obtained. The performance parameters of the CuO-SiNWs/GCE, fCuO/GCE, SiNWs/GCE, and archetype sensors from some other reports are listed in Table 1.

The ability of antiinterference is of crucial importance for the development of reliable H_2O_2 sensors because real samples may

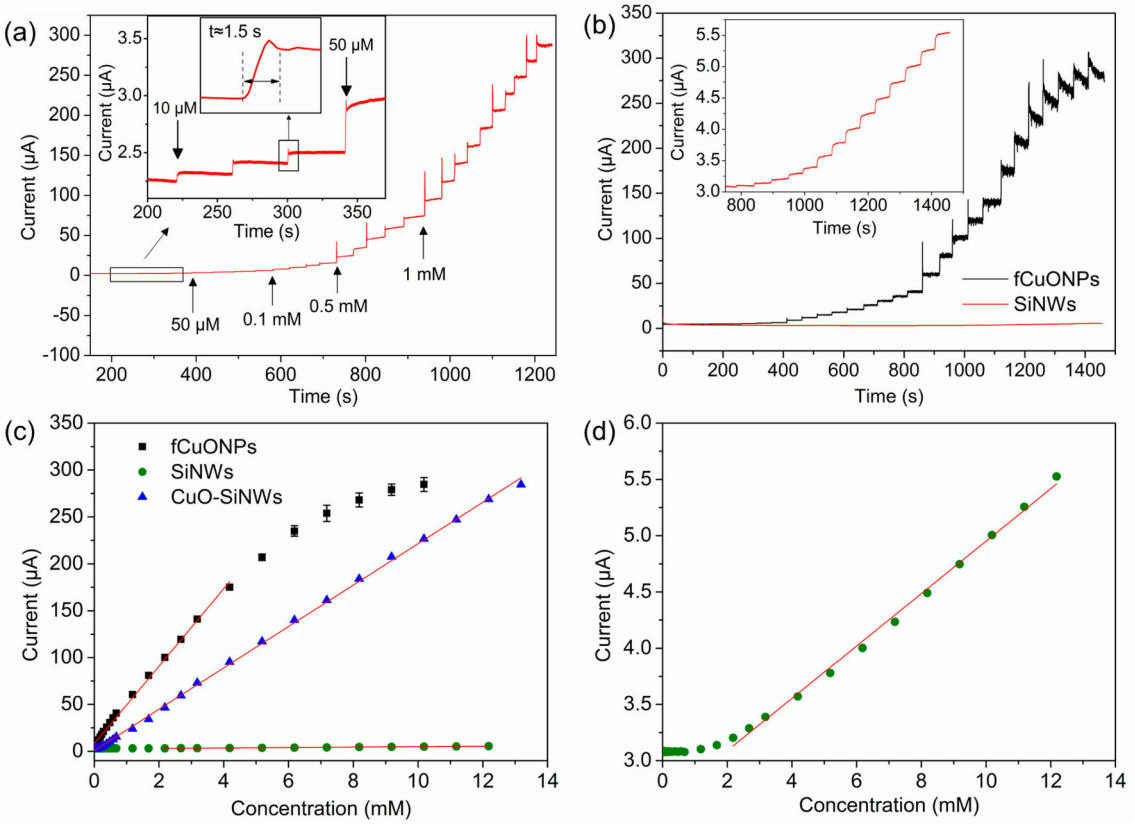

Figure 8. Current response of the (a) CuO-SiNWs/GCE and (b) fCuONPs/GCE and SiNWs/GCE to the successive addition of H_2O_2. The insets of parts a and b of Figure 7 respectively show current curves of the CuO-SiNWs/GCE at low concentrations and the SiNWs/GCE after an analyte concentration of 1.18 mM was reached. (c) Calibration plots of the three electrodes. (d) Magnified calibration plot of the SiNWs/GCE with considerably low sensitivity.

Table 1. Comparison of the Nonenzymatic H_2O_2 Detection Performance

electrode material	sensitivity (μA/mM)	linear range (mM)	detection limit (μM)	ref
CuO-SiNWs	22.27	0.01−13.18	1.6	this work
fCuONPs	41.34	0.01−4.18	2.5	this work
SiNWs	0.233	2.18−12.18	338	this work
CuONF-MWCNTs[a]	302.5	0.5−82	0.16	10
Cu_2O-rGO[b]	20.7	0.03−12.8	21.7	6
Pd-CNFs[c]	4.15	0.0002−0.02	0.2	35
Cu_2O NCs/GNs[d]	not available	0.3−7.8	20.8	36
AgNRs/rGO[e]	not available	0.1−70	2.04	37
PBI-BA-Gs[f]	207.0	0.025−5	3.1	38
N-doped CNTs[g]	24.5	0.00176−0.139	0.37	39
Ag-UTPNSs[h]	4.477	0.0193−90	0.57	40

[a]CuONF-MWCNTs, CuO nanoflower multiwalled C nanotubes. [b]Cu_2O-rGO, Cu_2O-reduced graphene oxide. [c]Pd-CNFs, Pd nanoparticle C nanofibers. [d]Cu_2O NCs/GNs, Cu_2O nanocubes/graphene nanosheets. [e]AgNRs/rGO, Ag nanorods/reduced graphene oxide. [f]PBI-BA/Gs, poly[*N*-(1-onebutyric acid)benzimidazole]/graphene sheets. [g]N-doped CNTs, nitrogen-doped C nanotubes. [h]Ag-UTPNSs, polypyrrole nanosheets decorated with Ag nanoparticles.

contain other electroactive species such as UA, AA, and glucose (Glu). We investigated the selectivity of the CuO-SiNWs/GCE by introducing the mentioned three possible interference species. In Figure 9, the successive addition of 0.2 mM Glu, 0.1 mM UA,

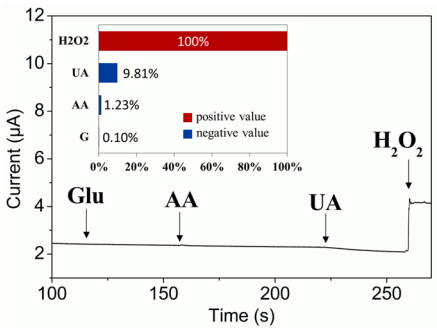

Figure 9. Antiinterference test via an amperometric *i*−*t* test with 0.2 mM Glu, 0.2 mM AA, and 0.1 mM UA in 0.1 M PBS (pH = 7.0) under stirring. The inset compares the current response of interference and the target analyte.

and 0.2 mM AA was performed and no major current change was observed for each addition. When 0.1 mM H_2O_2 was added, an evident current response was generated. Percentages of interference-induced current response compared to a 0.1 mM target analyte were +0.10%, −1.23%, and −9.81% for Glu, AA, and UA, respectively, which were all acceptable. This confirms CuO-SiNWs/GCE as a target-selective nonenzymatic sensor for H_2O_2 detection.

The reproducibility and long-term stability of the CuO-SiNWs/GCE were explored by measuring the current response

toward 200 μM H_2O_2. The relative standard deviation was calculated to be 2.94% (n = 10), confirming the good reproducibility necessary for repeated use. The CuO-SiNWs/GCE was left under an ambient environment after a test, and 14 days later, it maintained 81.6% of its initial response toward the identical concentration of the analyte, which ascertained its eligible long-term stability.

CONCLUSION

In summary, integration of well-dispersed CuO nanoparticles onto SiNW was realized via a precursor-mediated strategy. The SiNW arrays were prepared by metal-assisted chemical etching and were employed as the carrier for the electrocatalyst. Cu nanoparticles were grown as the precursor and were attached to SiNW through electroless deposition for the ensuing dry oxidation treatment. The successful formation of CuO nanoparticles on SiNWs was confirmed by microscopy combined with XRD. The GCE modified with CuO-SiNWs exhibited a satisfying performance for nonenzymatic H_2O_2 detection with a rapid response, a sensitivity of 22.27 μA/mM, and a detection limit of 1.6 μM according to a signal-to-noise ratio of 3. Besides, the CuO-SiNWs/GCE demonstrated an antiinterference ability against UA, AA, and Glu. To analyze the respective role of each component in the CuO-SiNWs, control tests via CV were carried out, which showed that the electrocatalytic activity toward H_2O_2 reduction was from the CuO electrocatalyst and SiNW only served as supporting backbones. Despite the negligible contribution to the current response from direct electrocatalysis, SiNW led to mitigated conglomeration of the CuO electrocatalyst and the favorable nanostructure for better analyte diffusion and electron transfer from the modified GCE to the electrocatalyst. Higher efficiency of electrocatalyst usage and better linearity compared to the counterpart without employing a SiNW carrier therefore resulted. Finally, the synthetic strategy proposed here provides a broadened scope for assembling nanosized metal oxides on the SiNW to generate functional nanocomposites for chemical sensing as well as other applications.

ASSOCIATED CONTENT

Supporting Information

Experimental details of the synthesis of free CuO nanoparticles by a solid-phase reaction, XRD and TEM characterization of the free CuO nanoparticles, construction of control groups of fCuONPs/GCE and SiNWs/GCE, CV of fCuONPs/GCE, thermodynamic calculation to prove the impossibility for the formation of Cu_2O, amperometric i–t test on interference from other electroactive species at an applied potential of −0.6 V, and additional TEM images of CuO-SiNW. This material is available free of charge via the Internet at http://pubs.acs.org.

AUTHOR INFORMATION

Corresponding Authors

*Tel: +86-21-64252022. Fax: +86-21-64250624. E-mail: yhzhu@ecust.edu.cn.

*Tel: +86-21-64252022. Fax: +86-21-64250624. E-mail: czli@ecust.edu.cn.

Notes

The authors declare no competing financial interest.

ACKNOWLEDGMENTS

This work was supported by the National Natural Science Foundation of China (Grants 21236003, 21206042, 20925621, and 21176083), the Basic Research Program of Shanghai (Grants 13NM1400700 and 13NM1400701), the Fundamental Research Funds for the Central Universities, and the Shanghai Leading Academic Discipline Project (Project B502).

REFERENCES

(1) Jia, W.; Guo, M.; Zheng, Z.; Yu, T.; Wang, Y.; Rodriguez, E. G.; Lei, Y. Vertically Aligned CuO Nanowires Based Electrode for Amperometric Detection of Hydrogen Peroxide. *Electroanalysis* **2008**, *20*, 2153–2157.

(2) Giorgio, M.; Trinei, M.; Migliaccio, E.; Pelicci, P. G. Hydrogen Peroxide: A Metabolic By-product or A Common Mediator of Ageing Signals? *Nat. Rev. Mol. Cell Biol.* **2007**, *8*, 722–728.

(3) Hua, M.-Y.; Lin, Y.-C.; Tsai, R.-Y.; Chen, H.-C.; Liu, Y.-C. A Hydrogen Peroxide Sensor Based on a Horseradish Peroxidase/polyaniline/carboxy-functionalized Multiwalled Carbon Nanotube Modified Gold Electrode. *Microchim. Acta* **2011**, *56*, 9488–9495.

(4) Munge, B. S.; Dowd, R. S.; Krause, C. E.; Millord, L. N. Ultrasensitive Hydrogen Peroxide Biosensor Based on Enzyme Bound to Layered Nonoriented Multiwall Carbon Nanotubes/Polyelectrolyte Electrodes. *Electroanalysis* **2009**, *21*, 2241–2248.

(5) Huang, K.-J.; Niu, D.-J.; Liu, X.; Wu, Z.-W.; Fan, Y.; Chang, Y.-F.; Wu, Y.-Y. Direct Electrochemistry of Catalase at Amine-functionalized Graphene/gold Nanoparticles Composite Film for Hydrogen Peroxide Sensor. *Microchim. Acta* **2011**, *56*, 2947–2953.

(6) Xu, F.; Deng, M.; Li, G.; Chen, S.; Wang, L. Electrochemical Behavior of Cuprous Oxide–Reduced Graphene Oxide Nanocomposites and Their Application in Nonenzymatic Hydrogen Peroxide Sensing. *Microchim. Acta* **2013**, *88*, 59–65.

(7) Narang, J.; Chauhan, N.; Pundir, C. A Non-enzymatic Sensor for Hydrogen Peroxide Based on Polyaniline, Multiwalled Carbon Nanotubes and Gold Nanoparticles Modified Au Electrode. *Analyst* **2011**, *136*, 4460–4466.

(8) Xiao, F.; Zhao, F.; Zhang, Y.; Guo, G.; Zeng, B. Ultrasonic Electrodeposition of Gold–platinum Alloy Nanoparticles on Ionic Liquid–chitosan Composite Film and Their Application in Fabricating Nonenzyme Hydrogen Peroxide Sensors. *J. Phys. Chem. C* **2008**, *113*, 849–855.

(9) Liao, F.; Cheng, L.; Li, J.; Shao, M.; Wang, Z.; Lee, S.-T. An Effective Oxide Shell-protected Surface-enhanced Raman Scattering (SERS) Substrate: the Easy Route to Ag@AgxO–silicon Nanowire Films via Surface Doping. *J. Mater. Chem. C* **2013**, *1*, 1628–1632.

(10) Meher, S. K.; Rao, G. R. Archetypal Sandwich-structured CuO for High Performance Non-enzymatic Sensing of Glucose. *Nanoscale* **2013**, *5*, 2089–2099.

(11) Zhang, K.; Zhang, N.; Cai, H.; Wang, C. A Novel Non-enzyme Hydrogen Peroxide Sensor Based on An Electrode Modified with Carbon Nanotube-wired CuO Nanoflowers. *Microchim. Acta* **2012**, *176*, 137–142.

(12) Ahmad, R.; Vaseem, M.; Tripathy, N.; Hahn, Y.-B. Wide Linear-Range Detecting Nonenzymatic Glucose Biosensor Based on CuO Nanoparticles Inkjet-Printed on Electrodes. *Anal. Chem.* **2013**, *85*, 10448–10454.

(13) Hahn, Y. B.; Ahmad, R.; Tripathy, N. Chemical and biological sensors based on metal oxide nanostructures. *Chem. Commun.* **2012**, *48*, 10369–10385.

(14) Chen, W.; Cai, S.; Ren, Q.-Q.; Wen, W.; Zhao, Y.-D. Recent Advances in Electrochemical Sensing for Hydrogen Peroxide: A Review. *Analyst* **2012**, *137*, 49–58.

(15) Shuai, D.; Choe, J. K.; Shapley, J. R.; Werth, C. J. Enhanced Activity and Selectivity of Carbon Nanofiber Supported Pd Catalysts for Nitrite Reduction. *Environ. Sci. Technol.* **2012**, *46*, 2847–2855.

(16) Bajpai, R.; Roy, S.; Rafiee, J.; Koratkar, N.; Misra, D. Graphene Supported Nickel Nanoparticle as A Viable Replacement for Platinum in Dye Sensitized Solar Cells. *Nanoscale* **2012**, *4*, 926–930.

(17) Sun, K.; Jing, Y.; Li, C.; Zhang, X.; Aguinaldo, R.; Kargar, A.; Madsen, K.; Banu, K.; Zhou, Y.; Bando, Y. 3D Branched Nanowire Heterojunction Photoelectrodes for High-efficiency Solar Water Splitting and H_2 Generation. *Nanoscale* **2012**, *4*, 1515−1521.
(18) Ryu, S.-W.; Kim, C.-H.; Han, J.-W.; Kim, C.-J.; Jung, C.; Park, H. G.; Choi, Y.-K. Gold Nanoparticle Embedded Silicon Nanowire Biosensor for Applications of Label-free DNA Detection. *Biosens. Bioelectron.* **2010**, *25*, 2182−2185.
(19) He, Y.; Su, S.; Xu, T.; Zhong, Y.; Zapien, J. A.; Li, J.; Fan, C.; Lee, S.-T. Silicon Nanowires-based Highly-efficient SERS-active Platform for Ultrasensitive DNA Detection. *Nano Today* **2011**, *6*, 122−130.
(20) Yu, H.; Li, X.; Quan, X.; Chen, S.; Zhang, Y. Effective Utilization of Visible Light (including $\lambda > 600$ nm) in Phenol Degradation with p-silicon Nanowire/TiO_2 Core/shell Heterojunction Array Cathode. *Environ. Sci. Technol.* **2009**, *43*, 7849−7855.
(21) Shi, J.; Hara, Y.; Sun, C.; Anderson, M. A.; Wang, X. Three-dimensional High-density Hierarchical Nanowire Architecture for High-performance Photoelectrochemical Electrodes. *Nano Lett.* **2011**, *11*, 3413−3419.
(22) Hwang, Y. J.; Boukai, A.; Yang, P. High Density n-Si/n-TiO_2 Core/shell Nanowire Arrays with Enhanced Photoactivity. *Nano Lett.* **2008**, *9*, 410−415.
(23) Pu, Y.-C.; Wang, G.; Chang, K.-D.; Ling, Y.; Lin, Y.-K.; Fitzmorris, B. C.; Liu, C.-M.; Lu, X.; Tong, Y.; Zhang, J. Z. Au Nanostructure-Decorated TiO_2 Nanowires Exhibiting Photoactivity Across Entire UV−visible Region for Photoelectrochemical Water Splitting. *Nano Lett.* **2013**, *13*, 3817−3823.
(24) Collins, G.; Holmes, J. D. Chemical Functionalisation of Silicon and Germanium Nanowires. *J. Mater. Chem.* **2011**, *21*, 11052−11069.
(25) Fang, C.; Agarwal, A.; Widjaja, E.; Garland, M. V.; Wong, S. M.; Linn, L.; Khalid, N. M.; Salim, S. M.; Balasubramanian, N. Metallization of Silicon Nanowires and SERS Response From a Single Metallized Nanowire. *Chem. Mater.* **2009**, *21*, 3542−3548.
(26) Zhang, M. L.; Peng, K. Q.; Fan, X.; Jie, J. S.; Zhang, R. Q.; Lee, S. T.; Wong, N. B. Preparation of Large-area Uniform Silicon Nanowires Arrays Through Metal-assisted Chemical Etching. *J. Phys. Chem. C* **2008**, *112*, 4444−4450.
(27) Guo, Z.; Seol, M.-L.; Kim, M.-S.; Ahn, J.-H.; Choi, Y.-K.; Liu, J.-H.; Huang, X.-J. Hollow CuO Nanospheres Uniformly Anchored on Porous Si Nanowires: Preparation and Their Potential Use as Electrochemical Sensors. *Nanoscale* **2012**, *4*, 7525−7531.
(28) Ozdemir, B.; Kulakci, M.; Turan, R.; Unalan, H. E. Effect of Electroless Etching Parameters on the Growth and Reflection Properties of Silicon Nanowires. *Nanotechnology* **2011**, *22*, 155606.
(29) Wang, X. L.; Han, W. Q. Graphene Enhances Li Storage Capacity of Porous Single-crystalline Silicon Nanowires. *ACS Appl. Mater. Interfaces* **2010**, *2*, 3709−3713.
(30) Huang, X.; Guo, C.; Zuo, J.; Zheng, N.; Stucky, G. D. An Assembly Route to Inorganic Catalytic Nanoreactors Containing Sub-10-nm Gold Nanoparticles with Anti-Aggregation Properties. *Small* **2009**, *5*, 361−365.
(31) Zong, J.; Zhu, Y.; Yang, X.; Shen, J.; Li, C. Synthesis of Photoluminescent Carbogenic Dots Using Mesoporous Silica Spheres as Nanoreactors. *Chem. Commun.* **2011**, *47*, 764−766.
(32) Su, S.; He, Y.; Song, S.; Li, D.; Wang, L.; Fan, C.; Lee, S. A Silicon Nanowire-based Electrochemical Glucose Biosensor with High Electrocatalytic Activity and Sensitivity. *Nanoscale* **2010**, *2*, 1704−1707.
(33) Yin, J.; Qi, X.; Yang, L.; Hao, G.; Li, J.; Zhong, J. A Hydrogen Peroxide Electrochemical Sensor Based on Silver Nanoparticles Decorated Silicon Nanowire Arrays. *Electrochim. Acta* **2011**, *56*, 3884−3889.
(34) Ahmad, R.; Tripathy, N.; Hahn, Y. B. Highly sensitive hydrazine chemical sensor based on ZnO nanorods field-effect transistor. *Chem. Commun.* **2014**, *50*, 1890−1893.
(35) Huang, J.; Wang, D.; Hou, H.; You, T. Electrospun Palladium Nanoparticle-Loaded Carbon Nanofibers and Their Electrocatalytic Activities towards Hydrogen Peroxide and NADH. *Adv. Funct. Mater.* **2008**, *18*, 441−448.
(36) Liu, M.; Liu, R.; Chen, W. Graphene Wrapped Cu_2O Nanocubes: Non-enzymatic Electrochemical Sensors for the Detection of Glucose and Hydrogen Peroxide with Enhanced Stability. *Biosens. Bioelectron.* **2013**, *45*, 206−212.
(37) Yu, B.; Feng, J.; Liu, S.; Zhang, T. Preparation of Reduced Graphene Oxide Decorated with High Density Ag Nanorods for Non-enzymatic Hydrogen Peroxide Detection. *RSC Adv.* **2013**, *3*, 14303−14307.
(38) Hua, M.-Y.; Chen, H.-C.; Tsai, R.-Y.; Leu, Y.-L.; Liu, Y.-C.; Lai, J.-T. Synthesis and Characterization of Carboxylated Polybenzimidazole and Its Use as A Highly Ssensitive and Selective Enzyme-free H_2O_2 Sensor. *J. Mater. Chem.* **2011**, *21*, 7254−7262.
(39) Xu, X.; Jiang, S.; Hu, Z.; Liu, S. Nitrogen-doped Carbon Nanotubes: High Electrocatalytic Activity Toward the Oxidation of Hydrogen Peroxide and Its Application for Biosensing. *ACS Nano* **2010**, *4*, 4292−4298.
(40) Mahmoudian, M.; Alias, Y.; Basirun, W.; Ebadi, M. Preparation of Ultra-thin Polypyrrole Nanosheets Decorated with Ag Nanoparticles and Their Application in Hydrogen Peroxide Detection. *Electrochim. Acta* **2012**, *72*, 46−52.